Energy 186 (2019) 115865

Contents lists available at ScienceDirect

Energy

journal homepage: www.elsevier.com/locate/energy

Optimization of process parameters for torrefaction of *Acacia nilotica* using response surface methodology and characteristics of torrefied biomass as upgraded fuel

Satyansh Singh, Jyoti Prasad Chakraborty*, Monoj Kumar Mondal

Department of Chemical Engineering and Technology, Indian Institute of Technology (Banaras Hindu University), Varanasi, 221 005, Uttar Pradesh, India

ARTICLE INFO

Article history:
Received 7 January 2019
Received in revised form
16 June 2019
Accepted 1 August 2019
Available online 6 August 2019

Keywords:
Acacia nilotica
Torrefaction
Optimization
Response surface methodology
Energy yield

ABSTRACT

The process parameters (temperature, residence time and heating rate) for torrefaction of *Acacia nilotica* in a fixed-bed reactor were optimized using response surface methodology. Maximum higher heating value and energy yield, both at the same time, were obtained at 252 °C, 60 min residence time, and 5 °C/min heating rate. Both the parameters were highly influenced by temperature; whereas residence time and heating rate had minimal impact. The torrefied biomass obtained at optimum condition was characterized by proximate and ultimate analysis, thermogravimetric analysis, Fourier transform infrared spectroscopy and scanning electron microscopy. Moisture content, H/C ratio and O/C ratio decreased by 73.23, 52.94, and 46.22%, respectively; while fixed carbon and higher heating value increased by 75.54 and 18.62%, respectively, as compared to raw biomass. Fuel properties such as fuel ratio increased by 87.39%, while combustibility index and volatile ignitability decreased by 83.32 and 22.71%, respectively. Flow properties such as angle of repose, Hausner ratio, Carr compressibility index and cohesion coefficient decreased by 8.04, 6.20, 22.48 and 12.5%, respectively. Enhanced fuel and flow properties make torrefied biomass a suitable feedstock for pyrolysis and gasification and optimization of this process may facilitate scale-up and reduce operational cost.

1. Introduction

The challenges associated with fossil fuels during energy production such as air pollution [1], global warming [2] and limited resources [3,4], force scientists and engineers to develop an interest towards renewable sources of energy. Solar, wind, geothermal, marine, hydrothermal and biomass come under the category of renewable energy resources [5]. Among the various renewable energy resources, biomass is having low cost, abundant worldwide [6] and easily accessible resource [7]. In addition, biomass is carbon neutral fuel [8] and has low sulphur and chlorine contents which reduce harmful emissions such as SO_x and NO_x during its application for bio-energy generation [9]. Thus, biomass as a sustainable source has great potential to be converted into solid, liquid and gaseous biofuels. In spite of large availability and easy access, some drawbacks are also associated with biomass like high moisture content [8], low calorific value, hydrophilic nature [10], low bulk density, and lower energy yield (EY) [8] which reduce the process efficiency along with increase in transportation, handling and storage cost [11]. Due to these shortcomings, biomass contributes around 10% of the total energy consumption of the world [12]. In this regard, it is better to upgrade biomass via some pretreatment step prior to use in thermochemical conversion processes. Among various pretreatment steps, torrefaction may be considered as a promising route to upgrade biomass [13].

In recent years, a lot of work has been carried out, while, many studies are currently going on regarding the utilization of biomass in producing alternative energy to fossil fuels [2,6]. Energy from biomass can be extracted through various techniques such as chemical, thermochemical and biological methods [10,14]. With respect to general thermochemical processes applied on biomass, most prominent one are torrefaction, pyrolysis, gasification, combustion [15], and hydrothermal liquefaction [3]. The most valuable products from pyrolysis and gasification of biomass are bio-oil and producer gas, respectively, while combustion of biomass is used to generate heat directly [15]. Torrefaction is used as a pretreatment step which produces high-quality solid biofuel as torrefied biomass (TB). This TB can be used in different thermochemical conversion

* Corresponding author.
E-mail address: jpc.che@iitbhu.ac.in (J.P. Chakraborty).

https://doi.org/10.1016/j.energy.2019.115865
0360-5442/

Nomenclature

Abbreviations

ANSI	American National Standards Institute
ANOVA	Analysis of variance
ASTM	American Society for testing and materials
AC	Ash content (wt %)
BET	Brunauer–Emmett–Teller
C	Cohesion coefficient
CCI	Carr compressibility index
CI	Combustibility index (MJ/kg)
CrI	Crystallinity index (%)
CHNS	Carbon Hydrogen Nitrogen Sulphur
db	Dry basis
d_{gm}	Geometric mean diameter (mm)
DTG	Differential thermogravimetry
d_i	Aperture diagonal of ith screen
d_{i-1}	Aperture diagonal of next larger screen
EY	Energy yield (%)
EDX	Energy dispersive X-ray (EDX)
FC	Fixed carbon (Wt %)
FR	Fuel ratio
FTIR	Fourier transform infrared spectroscopy
FWHM	Full width at half maximum
HHV	Higher heating value (MJ/kg)
HR	Hausner ratio
I_{002}	Crystalline intensity of diffraction plane (002)
I_{am}	Amorphous intensity of diffraction plane (002)
L_{002}	crystal size
M_i	Mass retained on ith screen (kg)
M_1	Initial mass of sample (kg)
M_{2i}	Mass of sample after ith day (kg)
m_g	Total mass of cylinder with sample (kg)
m_t	Total mass of cylinder with sample after tapping (kg)
m_c	Mass of empty cylinder
m_p	Mass of geometrical shape (kg)
P_1	Pressure after pressurizing the reference volume (Pa)
P_2	Pressure after including V_C (Pa)
RB	Raw biomass
SEM	Scanning electron microscope
TB	Torrefied biomass
TBX-Y-Z	Torrefied biomass at optimum condition
X	Optimum temperature
Y	Optimum residence time
Z	Optimum heating rate
TGA	Thermogravimetric analysis
V_p	Volume of biomass (m^3)
V_c	Sample cell volume (m^3)
V_R	Reference volume (m^3)
V_L	Volume of measuring cylinder (m^3)
XRD	X-Ray diffraction (XRD)

Greek letters

ρ_b	Bulk density (kg/m^3)
ρ_{Tb}	Tapped density (kg/m^3)
ρ_p	Particle density (kg/m^3)
k	Scherrer constant (0.90)
λ	X-ray wavelength (0.15406 nm)
β	FWHM of peak

processes like pyrolysis, gasification and combustion to increase the quality of products such as high-grade bio-oil [12] and producer gas [16] with lower harmful emission [17] during the process. Therefore, the overall efficiency of the thermochemical process can be increased by using TB [12].

Torrefaction is a mild thermochemical process, which occurs generally in temperature range of 200–300 °C under atmospheric pressure [18] in presence of inert atmosphere [13] or limited oxygen environment with a low heating rate (<50 °C/min) [18] with residence time less than 60 min [19]. In this temperature zone, almost complete degradation of hemicellulose takes place, whereas retaining most of the energy of biomass [12]. It removes both bound and unbound moisture content along with organic volatile matter mainly from hemicellulose and a small amount from cellulose and lignin [20]. Thus, TB contains cellulose and lignin in larger proportion than hemicellulose with higher carbon content, and lower H/C and O/C ratios [7]. Moreover, it has superior properties than raw biomass (RB) in terms of moisture content (MC), fixed carbon content (FC), HHV, hydrophobicity, EY and bulk density as suggested by many authors. Phanphanich et al. [21] investigated the torrefaction of pine wood chips and found that MC decreased from 6.69 to 2.57%, FC increased from 13.76 to 40.85%, HHV increased from 18.46 to 25.38 MJ/kg, H/C ratio decreased from 1.69 to 1.05% and EY was found to be 71% when torrefied at 300 °Cat a residence time of 30 min. Conag et al. [22] extensively investigated the influence of temperature on the bulk and tapped density of sugarcane bagasse and sugarcane leaves and found that with an increase in temperature during torrefaction, both bulk and tapped densities decreased. Chen et al. [23] studied the hygroscopic properties of TB and concluded that equilibrium moisture content decreased up to 35% when *Abies pectinata* was torrefied at 230 °C.

The process of torrefaction depends not only on structure of biomass (amount of cellulose, hemicellulose and lignin) and ash content [7] but also depends on the process parameters like temperature, heating rate, residence time [20], and particle size [12]. Chen et al. [24] suggested that torrefaction process is highly influenced by temperature rather than residence time. Generally, as the temperature increases during torrefaction, more volatiles are released due to the conversion of oxygen-containing compounds. The variation of solid yield and HHV of TB with residence time is marginal at a fixed temperature [20]. Mundike et al. [25] investigated torrefaction over lantana camara plant and found that at 280 °C, increase in residence time from 25 to 80 min, EY of TB decreases from 65.97% to 52.42%. Many such literatures are available showing the effect of temperature, residence time and heating rate, however, to the best of author's knowledge, very few work have been reported regarding optimum value of temperature, residence time and heating rate for torrefaction process for energy densification and energy utilization. In addition, characteristics of TB at optimum condition relative to RB have not been reported. Also, no work related to torrefaction of *Acacia nilotica* has been reported.

Response surface methodology (RSM) is one of the most prevalent and promising techniques to develop, improve, and optimize the process parameters and their interaction effect on the process with a minimum number of experiments. It was developed by Box and Wilson in 1951 [26]. It is a statistical and mathematical [27] technique having a multivariable non-linear model, which generally is used to optimize the process parameters. In it, a mathematical model is developed which, best fits the experimental data [28]. The optimum values of responses are obtained using developed model.

In this article, *Acacia nilotica* was chosen for torrefaction in a

laboratory scale fixed-bed reactor. *Acacia nilotica* (commonly known as Babool in India) trees are generally found in African, Australia and South East Asian countries. These trees are commonly found in waste and barren land having height around 5–20 m with dense braches and leaves canopy. In India, these are found usually in the northern part and annual production of *Acacia nilotica* pod is around 0.6 million metric tonnes [29]. Such a large production brings attention towards selection of *Acacia nilotica* for bio-energy production via thermochemical conversion. Meanwhile, torrefaction process depends on different parameters such as temperature, residence time and heating rate. Also, EY and HHV of solid product are important outcomes of the process. However, EY and HHV reflect opposite trend, when process parameters are varied during experiment. Thus, optimizing the process parameters and a balance between EY and HHV becomes quite important for energy densification and energy utilization. Optimization may reduce operational cost regarding scale-up of the process at industrial level. Thus considering TB as desired product from torrefaction, optimization of process parameters such as temperature, residence time and heating rate for HHV and EY of TB was performed using RSM. The ANOVA and regression analysis were used to study the fitness of developed model using central composite design technique. In addition, the characteristics of TB at optimized condition were tested using TGA, FTIR, XRD, BET, and SEM analysis and compared with RB. Moreover, the fuel characteristics like fuel ratio (FR), combustibility index (CI), volatile ignitability (VI), flow behavior through angle of repose, Hausner ratio (HR), Carr compressibility index (CCI), cohesion coefficient (C), moisture sorption ability and densities (bulk, tapped and particle) of RB and TB at optimized condition were also investigated.

2. Material and methods

2.1. Sample preparation

Acacia nilotica used in this work was collected from the village area nearer to Indian Institute of Technology (BHU), Varanasi. The collected wooden blocks were cut into smaller pieces using an axe and then fine particles were obtained using a cutting mill (Retsch model SM 300, Germany). Particle size between 0.7 and 1.25 mm was obtained by sieve screening analysis. Biomass was kept in sun light for one day to remove loose moisture. The sun-dried biomass sample was further dried overnight in a hot air oven maintained at 80 °C, before carrying out further analysis.

2.2. Experimental design using RSM

For optimization of parameters, RSM was used. A three-factor face central composite design, a kind of RSM technique was used to optimize the response in the process. The central composite design technique is well suited for fitting a quadratic surface, which usually works well for any process optimization. This technique is being widely used since it provides a minimum number of experimental run for optimizing the response variable and an easy way to estimate the interaction between different parameters. Assuming the experiments will be performed in a single day with one block, twenty experiments have to be performed, which may be derived from Eq. (1) [30], comprising eight factorial points (2^n), six axial points (2n) and six replicates at center points (n_c).

$$N = 2^n + 2n + n_c = 2^3 + 2(3) + 6 = 20 \quad (1)$$

where N is the total number of experiments that have to be performed, n is the number of independent variables and n_c is the number of replicates at central points.

The central point varies between 3 and 10 and it can be used to predict experimental error and reproducibility of data. Temperature (A), residence time (B) and heating rate (C) of range 220–280 °C, 20–60 min and 5–15 °C/min, respectively were selected as independent variables. Code −1, 0 and + 1 were the value of temperature (220, 250 and 280 °C), residence time (20 min, 40 min and 60 min) and heating rate (5, 10, and 15 °C/min). HHV and EY of TB were chosen as response and both the responses have to be maximized. The matrix of experimental design is given in Table S1. The experimentally calculated HHV and EY are incorporated in design expert software (Stat-Ease Design-Expert version-11) as the actual value. While predicted and residual values obtained by software. Data obtained from the experiments were used to optimize the selected parameter. The suggested mathematical model having highest polynomial degree was chosen from central composite design and also it should not be aliased [31].

Once the experiments have been performed, the response variables (HHV and EY of TB) were correlated with independent parameters (temperature, residence time and heating rate). The general relationship between response and independent variable is given as:

$$Y = f(X_1, X_2, X_3, \ldots\ldots, X_n) \quad (2)$$

where Y is the response variable, f is the function relating response to independent variable and X_1, X_2, X_3, … …. . X_n are the n independent variables which affect the response.

Following the second order polynomial equation as suggested by central composite design technique, the generalized form of second order polynomial equation is given as:

$$Y = b_0 + \sum_{i=1}^{k} b_i X_i + \sum_{i=1}^{k} b_{ij} X_i^2 + \sum_{i_{>j}}^{k} \sum_{j}^{k} b_{ij} X_i X_j \quad (3)$$

where i is the linear coefficient, j is the quadratic coefficients, b is the regression coefficient, k is the number of factors that were studied and optimized in the study.

The ANOVA and regression analysis were used to study the fitness of regression model at 95% confidence level using Design-Expert software. This analysis was used to check the deviation of mean. Set of experimental data were analyzed in accordance with several variables like p value, degree of freedom (DF), F value, determination coefficient (R^2), predicted determination of coefficient (R^2_{pred}) and adjusted determination of coefficient (R^2_{adj}) to check the statistical fitness of the model. From ANOVA, F and p values are used to examine the importance of terms appeared in the model equation. F value suggests that variation in responses can be demonstrated by regression equation, whereas, p value specifies, whether F value is large enough to ascertain statistical importance of the developed model. For that matter, p value for model should be less than 0.05 and p value for lack of fit test should be greater than 0.05 [26]. Three dimensional RSM plots and contour plots were incorporated to analyze the effect of each variable and their interaction with HHV and EY of TB.

2.3. Experimental setup and torrefaction procedure

The schematic diagram of the experimental setup is shown in Fig. S1 (available in the supplementary material). It consists of temperature controller unit and a fixed-bed reactor (Inner diameter = 2.5 cm, length = 80 cm) made up of quartz, split tube furnace (NSW-104 New Delhi), recirculating bath (Eyela CA-1112CE, Japan), and a counter-current condenser unit. In each experiment, 10 g of RB was loaded into the reactor on a support of ceramic wool. The

height of sample in the reactor was around 10 cm. A K- type thermocouple was inserted into the reactor for measuring the temperature of torrefaction. The tip of thermocouple just touched the upper surface of sample. The reactor was then purged by nitrogen gas (99.999% purity, Ashish Enterprise, Varanasi) at a flow rate of 45 mL/min using mass flow controller (Bronkhorst, Netherlands) for 30 min to remove oxygen trapped into the bed. Then, the furnace was turned on and heating rate was measured from control panel of furnace. The torrefaction of RB was carried out between 220 and 280 °C with residence time between 20 and 60 min and heating rate between 5 and 15 °C/min, following the experimental matrix given in Table S1. In each case, when the residence time was over, the furnace automatically started cooling. The solid residue (TB) was taken out of the reactor when room temperature reached. All the experiments were performed twice and average values were reported.

The products of torrefaction process are solid residue (TB), condensable liquid (bio-oil) and non-condensable (NC) gases. Generally, torrefaction is being used as a pre-treatment process to upgrade the quality of biomass which can be used as fuel in other thermochemical conversion processes like pyrolysis and gasification. Keeping this in mind, TB is considered as the main product in this study. The TB yield was calculated using Eq. (4).

$$\text{TB yield(wt\%)} = \frac{\text{Weight of TB(g)}}{\text{Weight of RB(g)}} \times 100 \tag{4}$$

Energy yield is a function of solid product yield and their HHV. EY can be calculated using Eq. (5).

$$\text{Energy yield} = (\text{TB yield}) \times \frac{\text{HHV}_{\text{db,TB}}}{\text{HHV}_{\text{db,RB}}} \tag{5}$$

2.4. Characteristics of raw and torrefied biomass

Proximate analysis of RB and TB was performed to find suitability of biomass for thermochemical conversion processes like pyrolysis and gasification. Moisture content (MC), ash content (AC) and volatile matter (VM) in weight percent were calculated according to standard methods ASTM E871, ASTM E1755 and ASTM E872, respectively. Fixed carbon (FC) was calculated by difference (100 − (% MC + % AC + % VM)). The elemental composition of RB and TB was measured by using CHNS analyzer (EURO EA3000, EURO VECTOR instrument and software, Italy). Oxygen content was calculated by difference (100 − (% C + % H + % N)). Bomb calorimeter (IKA, C-200 model, Germany) was used to estimate the HHV of RB and TB. All three types of densities (bulk, tapped, and particle) were calculated using Eqs. (6)–(8), by following standard method ASTM E873-82. For particles having an irregular shape, Eq. (9) [32] can be used to measure the volume of particles. The American National Standards Institute (ANSI) protocol was followed to calculate the size distribution of biomass. Biomass collected on each screen was weighed, once the shaking was over. The geometric mean diameter d_{gm} of biomass particle can be calculated using the relation mentioned by Cai et al. [33] in Eq. (10).

$$\text{Bulk density, } \rho_b(\text{kg}/\text{m}^3) = \frac{m_g - m_c}{V_L} \tag{6}$$

$$\text{Tapped density, } \rho_{Tb}(\text{kg}/\text{m}^3) = \frac{m_t - m_c}{V_L} \tag{7}$$

$$\text{Particle density, } \rho_p(\text{kg}/\text{m}^3) = \frac{m_p}{V_p} \tag{8}$$

$$V_p = V_c - V_R\left(\frac{P_1}{P_2} - 1\right) \tag{9}$$

$$d_{gm} = log^{-1}\left(\frac{\sum M_i . log\sqrt{d_i . d_{i-1}}}{\sum M_i}\right) \tag{10}$$

To estimate the usefulness of TB as solid fuel, some combustion indices are usually used such as fuel ratio, combustibility index and volatile ignitability. Combustion indices were calculated using Eqs. 11–13 as mentioned by Conag et al. [22].

$$\text{Fuel ratio} = \frac{FC_{db}}{VM_{db}} \tag{11}$$

$$\text{Combustibility index(MJ/kg)} = \frac{HHV_{db}}{FR} \times (115 - \text{Ash}_{\text{db}}) \times \frac{1}{105} \tag{12}$$

$$\text{Volatile ignitability(MJ/kg)} = \left[\frac{HHV_{db} - 0.338FC_{db}}{VM_{db} + MC_{db}}\right] \times 100 \tag{13}$$

The flow performance of biomass can be investigated through several parameters like angle of repose, cohesion coefficient, Hausner ratio and Carr compressibility index, [34]. Various methods have been reported for calculation of angle of repose like fixed funnel method, tilting box method and revolving cylinder method [33]. In present work, fixed funnel method (ASTM-C144) was used to calculate the angle of repose by using Eq. (14). Cohesion coefficient is a function of particle size and angle of repose of biomass which was calculated using correlation derived by Szalay et al. [35] (Eq. (15)). Hausner ratio is a function of tapped density and bulk density of biomass and was calculated using Eq. (16). Carr compressibility index is used to investigate the particulate interaction and flow behavior of material. It is a function of bulk density and tapped density of material and was calculated using Eq. (17).

$$\text{Angle of repose } (\theta) = \tan^{-1}\left(\frac{H}{R}\right) \text{ Where R} = D/2;\ \text{D is the diameter of cone at the base} \tag{14}$$

$$\text{Cohesion coefficient} = \frac{1}{2}d\left(\sqrt{\cos^2\theta + \frac{4\sin\theta}{d}} - \cos\theta\right) \tag{15}$$

$$\text{Hausner ratio} = \frac{\rho_{Tb}}{\rho_b} \tag{16}$$

$$\text{Carr compressibility index} = \left(1 - \frac{\rho_b}{\rho_{Tb}}\right) \times 100 \tag{17}$$

Brunauer–Emmett–Teller (BET) surface area of TB252-60-5 was determined on an ASAP 2020 adsorption apparatus (Micromeritics, USA). Thermogravimetric analysis of RB and TB252-60-5 was investigated to estimate mass loss characteristics using TGA (PerkinElmer STA 6000). The changes in chemical structure during torrefaction were investigated using Fourier transform infrared spectroscopy (Varian 1000, USA). Morphological characteristics and relative abundance of elements present on the surface of RB and TB252-60-5 were investigated using scanning electron microscopy

(JEOL JSM5410, Japan). The crystallinity of the RB and TB252-60-5 was investigated using X-ray diffractometer (mini flux II, Rigaku, Japan). The crystallinity index and crystal size were calculated using Eqs. (18) and (19). The behavior of RB and TB252-60-5 with respect to time and environment (average relative humidity of 60% ±3) was investigated. The percentage moisture absorbed was calculated using Eq. (20). The description for measurement of angle of repose, BET surface area, TGA, FTIR, XRD and moisture absorption test in detail are given in supplementary material (Procedure S1).

$$\mathrm{CrI}(\%) = \left(\frac{I_{002} - I_{am}}{I_{002}}\right) \times 100 \tag{18}$$

$$\mathrm{L}_{002} = \frac{k \times \lambda}{\beta \times \cos\theta} \tag{19}$$

$$\%\text{Moisture absorbed} = \frac{\mathrm{M}_{2i} - \mathrm{M}_1}{\mathrm{M}_1} \times 100 \quad \mathrm{i} = 1 \text{ to } 5 \text{ days} \tag{20}$$

3. Results and discussion

3.1. Solid product yield and EY

The fraction of each product depends on operating parameter like temperature, residence time, heating rate. Maximum and minimum solid yield (73.82% and 38.13%) were obtained at temperature (220 and 280 °C), residence time (20 and 60 min), and heating rate (5 °C/min), respectively. With increase in temperature during torrefaction, decomposition of hydroxyl group becomes more significant and results in release of larger amount of water vapour; hence, the fraction of condensable liquid increases with increase in temperature at a particular residence time and heating rate. Solid yield from torrefaction process also depends on type of biomass and their constituents. Biomass having more hemicellulose yields less solid char during torrefaction since degradation of hemicellulose takes place at relatively lower temperature than cellulose and lignin. EY gives an indication about the amount of energy preserved in biomass after torrefaction. The EY of TB decreases with temperature at constant residence time and heating rate. Maximum and minimum EY (76.35% and 49.72%) were obtained at temperature (220 and 280 °C), residence time (20 min), and heating rate (5 and 15 °C/min), respectively. As the residence time increases, the yield of liquid and non-condensable gases increased. At a fixed temperature and longer residence time, biomass is exposed for longer duration, hence, yield of liquid and gas enhanced. Higher residence time also favors the devolatilization reaction, which can increase the yields of liquid product and gases.

3.2. Response surface analysis for HHV and EY of torrefied biomass

The relation between experimental and predicted values of HHV and EY of TB are shown in Fig. 1 (a) and (b), respectively. It shows that both values are close to each other, indicating that the developed model is well suited to establish the relation between dependent and independent variables during torrefaction process. This relationship can also be justified by the value of correlation coefficient (R^2), which varies between zero to one. The value of coefficient close to one indicates lesser error in developed model. For present model, values of correlation coefficients for HHV and EY of TB are 0.9957 and 0.9921, respectively, indicating a good correlation between independent and dependent variables.

The relation between dependent parameter (HHV) and independent parameters (temperature (A), residence time (B), and heating rate (C)) obtained in this study is:

$$\mathrm{Y_{HHV}(MJ/kg)} = +21.2581 - 0.7266\mathrm{A} - 0.0284\mathrm{B} - 0.0277\mathrm{C} + 0.0001\mathrm{AB} + 0.0001\mathrm{AC} - 0.00008\mathrm{BC} + 0.00002\mathrm{A}^2 - 0.0003\mathrm{B}^2 - 0.0002\mathrm{C}^2$$

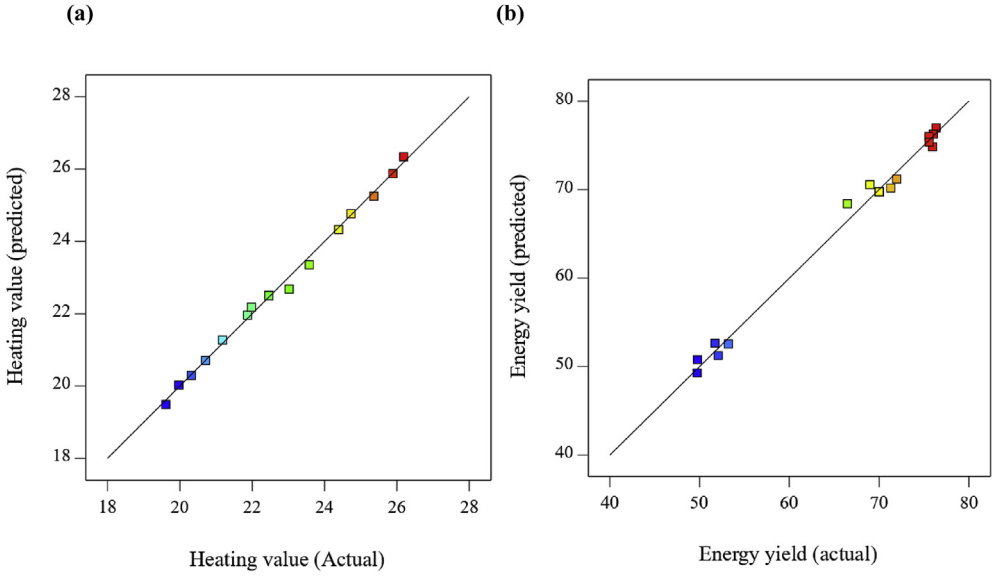

Fig. 1. Relationship between actual and predicted values of model (a) HHV and (b) EY.

The statistical analysis of HHV is given in Table 1. The significance of each independent variable on the response can be analyzed using F-value and p-value. For a significant model, the p-value should be less than 0.05 and F- value should be large. For present model, p-value and F-values are <0.0001 and 256.54 for HHV, suggesting that the developed model is applicable. The p-value and F-value of model can also be used to compare the linear term (A, B, C), interaction term (AB, AC, BC), and quadratic term (A^2, B^2, C^2). For HHV of TB linear term (A, B and C) and quadratic term (A^2) are significant having p-value <0.0001, <0.0001 0.0009, and 0.0270 respectively. The F-value of all the significant terms (A, B, C, and A^2) is 2099.53, 166.72, 21.56 and 6.70, respectively. It can be concluded that for HHV of TB, temperature has a larger effect on the process than residence time and heating rate.

Three dimensional (3D) and contour plots of response at optimized condition were obtained in this study to verify the dependence of HHV of TB with different process parameters like temperature, residence time and heating rate (Fig. 2). In case of three independent variables, it is not possible to show the effect of all variable on the response simultaneously. Hence the effect of two variables keeping third as constant is shown in this study. Fig. 2 (a and b) show the 3D and contour plots for variation of HHV of TB with respect to temperature and residence time. It can be seen that at a constant heating rate of 5 $^{\circ}C$/min, the HHV of TB increases up to a maximum value, with increase in temperature and residence time. Similar results can be obtained in case of variation of HHV of TB with temperature and heating rate at a constant residence time of 60 min (Fig. 2 (c and d)). It can be concluded that maxima of HHV of TB can be obtained in case of higher temperature, residence time and heating rate. A flat 3D surface can be seen in Fig. 2 (e and f) confirming that HHV of TB does not vary too much with an increase in residence time and heating rate at particular temperature (250 $^{\circ}C$). In can be mentioned that torrefaction is more temperature driven process than residence time and heating rate. Thus, properties like HHV and EY are highly dependent on temperature than the residence time and heating rate. With an increase in temperature, relative increase in carbon content and a decrease in oxygen content lead to increase in HHV of biomass.

The statistical analysis for EY is given in Table 1. For developed model in case of EY, p-value and F-value are <0.0001 and 139.88, suggesting that developed model is significant. For EY of TB, linear term (A and C), and quadratic term (A^2) are significant, having p-values <0.0001, 0.0380, and <0.0001, respectively. In case of EY, the F values for significant terms (A, C, and A^2) are 1103.88, 5.71, and 89.57, respectively. The dependency related to temperature is similar to HHV; however EY has the different trend relative to residence time and heating rate. In case of EY, the process is more dependent on heating rate than residence time.

Fig. 3 shows the 3D and contour plots for response EY at optimized condition with respect to independent variables. Fig. 3 (a and b) and (c and d) show the coupled effect of temperature-residence time at constant heating rate of 5 $^{\circ}C$/min and temperature-heating rate at constant residence time of 60 min, respectively on EY. It was found that the maximum value of EY can be obtained at lower temperature, residence time and heating rate during torrefaction process. A flat 3D surface can be seen confirming that EY of TB does not vary too much with an increase in residence time and heating rate at a particular temperature (Fig. 3 (e and f)). At lower temperature, the degradation of hemicellulose is less and almost insignificant for cellulose and lignin [12] due to lower rate of

Table 1
ANOVA for quadratic model of response: HHV and EY.

Source	Sum of square	Degree of freedom	Mean of square	F-value	p-value	Remark
HHV						
Model	67.47	9	7.50	256.54	<0.0001	Significant
A-Temperature	61.36	1	61.36	2099.53	<0.0001	
B-Residence time	4.87	1	4.87	166.72	<0.0001	
C-Heating rate	0.6300	1	0.6300	21.56	0.0009	
AB	0.0528	1	0.0528	1.81	0.2085	
AC	0.0045	1	0.0045	0.1544	0.7026	
BC	0.0006	1	0.0006	0.0210	0.8878	
A^2	0.1958	1	0.1958	6.70	0.0270	
B^2	0.0634	1	0.0634	2.17	0.1716	
C^2	0.0147	1	0.0147	0.5040	0.4940	
Residual	0.2922	10	0.0292			
Lack of Fit	0.2922	5	0.0584	4.58	0.0569	
Pure Error	0.0000	5	0.0000			
Cor Total	67.76	19				
R^2 0.9957	Adjusted R^2 0.9918			Predicted R^2 0.9681		
EY						
Model	1724.53	9	191.61	139.88	<0.0001	Significant
A-Temperature	1512.10	1	1512.10	1103.88	<0.0001	
B-Residence time	0.9912	1	0.9912	0.7236	0.4149	
C-Heating rate	7.82	1	7.82	5.71	0.0380	
AB	0.3121	1	0.3121	0.2279	0.6434	
AC	0.6280	1	0.6280	0.4584	0.5137	
BC	1.76	1	1.76	1.29	0.2831	
A^2	122.70	1	122.70	89.57	<0.0001	
B^2	3.44	1	3.44	2.51	0.1440	
C^2	0.5822	1	0.5822	0.4250	0.5292	
Residual	13.70	10	1.37			
Lack of Fit	13.70	5	2.74	6.68	0.0647	
Pure Error	0.0000	5	0.0000			
Cor Total	1738.23	19				
R^2 0.9921	Adjusted R^2 0.9850			Predicted R^2 0.9244		

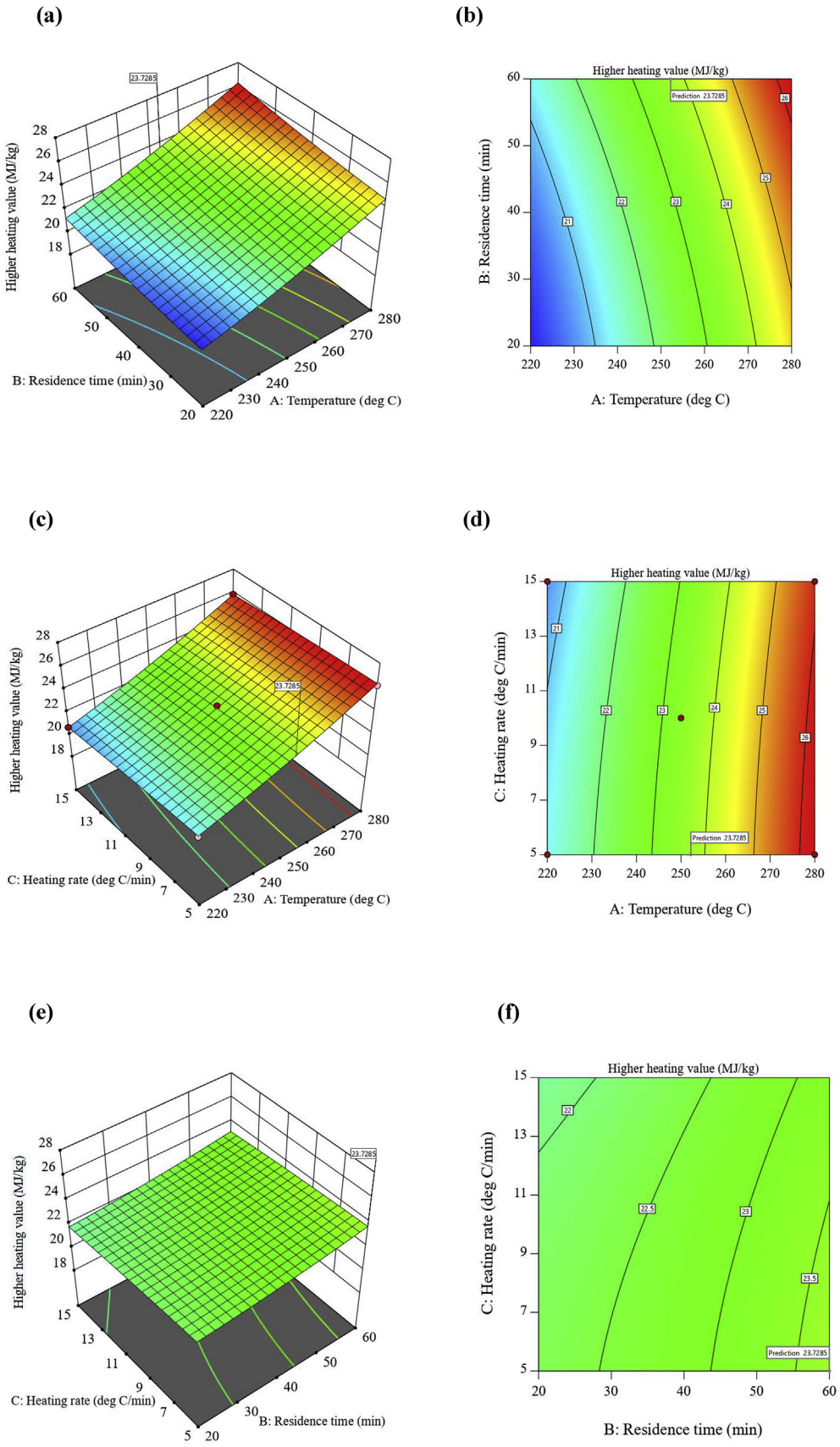

Fig. 2. Three dimensional response surface and contour plots of HHV showing the effect of (a) and (b) temperature and residence time; (c) and (d) temperature and heating rate; (e) and (f) heating rate and residence time. For EY, relation between dependent and independent (temperature, residence time and heating rate) variable is as follows.

$$Y_{EY}(\%) = +3.3065A - 0.3372B + 0.4703C + 0.0003AB - 0.0018AC + 0.0046BC - 0.0074A^2 + 0.0027B^2 - 0.0184C^2 - 287.3708$$

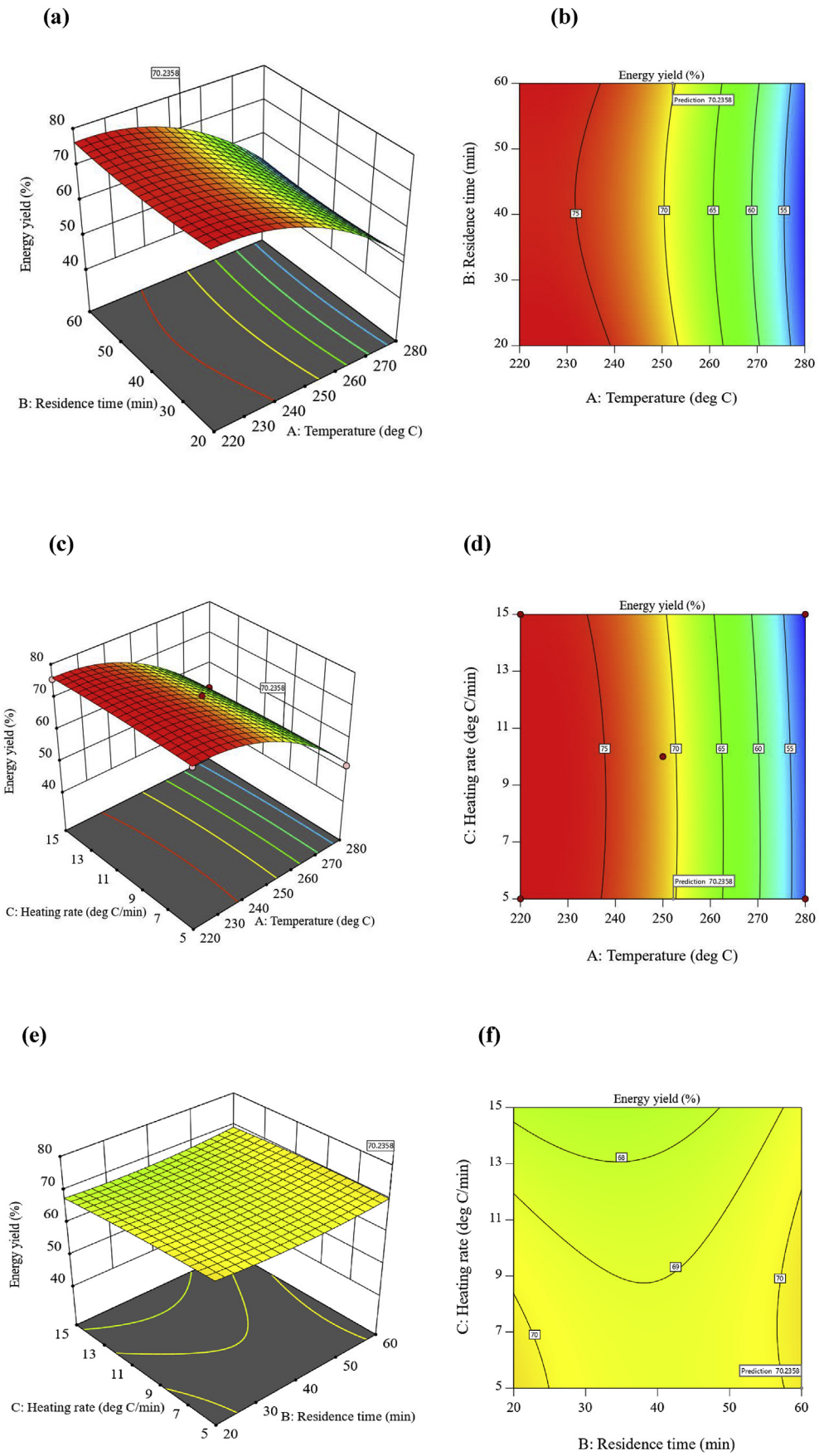

Fig. 3. Three dimensional response surface and contour plots of EY showing the effect of (a) and (b) temperature and residence time; (c) and (d) temperature and heating rate; (e) and (f) heating rate and residence time.

devolatilization. Hence, mass loss is very small.

3.3. Optimization of HHV and EY of torrefied biomass

Twenty experiments have been performed according to the experimental matrix given in Table S1. The maximum HHV (25.87 MJ/kg) of TB was found at 280 °C, 57 min residence time and 5 °C/min heating rate (Table S2). On the other hand, maximum EY (75.14%) was obtained at 220 °C, 20 min residence time and 10 °C/min heating rate (Table S2). It is evident that both HHV and EY attain maximum value at different set of conditions. It may be mentioned that EY indicates energy densification, whereas HHV refers to the direct utilization potential of TB as solid fuel. Maximum HHV at minimum EY would be beneficial for using TB as solid fuel. While maximum EY at minimum HHV would be required in case of biomass densification. In the present study, there was a need to maximize both HHV and EY. As predicted by RSM, the maximum value of HHV and EY are 23.73 MJ/kg and 70.20%, respectively, obtained at 252 °C, 60 min residence time and 5 °C/min heating rate. For validating these data, experiments were performed and it can be seen that the error is less than 2% (Table S2). This clearly suggests that the developed model is in good agreement with the experimental findings.

3.4. Physical and chemical properties of raw and torrefied biomass

The proximate and ultimate analyses data along with HHV and EY at optimized condition are presented in Table 2, which clearly shows that MC and VM both decreased as the temperature increased during torrefaction. MC for RB is 6.24%, while 1.67% TB252-60-5. Besides, the VM also decreased from 80.36% for RB to 44.78% for TB252-60-5. The AC of biomass increased from 0.65% for RB to 1.42% for TB252-60-5. Ash has strong affinity to deposit in the boiler, pyrolyzer, and gasifier [33]. So it will be helpful to know the physical and chemical characteristic of ash to prevent such problems of deposition. The FC increased from 12.75% for RB to 52.13% for TB252-60-5. This increase in FC and AC was observed during torrefaction because as the temperature increases, rate of devolatilization of (water vapour, methane, ethane, and other lighter hydrocarbon) from biomass also increases which results in relative decrease in MC and VM and relative increase in FC and AC. During torrefaction, loss of hydrogen and oxygen are more compared to the loss of carbon. The relative increase in the carbon content of biomass during torrefaction is responsible for higher HHV. The HHV obtained for RB, and TB252-60-5 are 19.31, and 24.06 MJ/kg, respectively. These results are in good agreement with the published literature for similar feedstock.

Table 2
Characteristics of RB and TB252-60-5.

Analysis	RB	TB252-60-5
MC (wt%)	6.24	1.67
AC (wt%)	0.65 (0.69)	1.42 (1.44)
VM (wt%)	80.36 (85.70)	44.78 (44.54)
FC (wt%)	12.75 (13.59)	52.13 (53.01)
O/C	1.09	0.60
H/C	0.17	0.08
HHV (MJ/kg)	19.31 (20.59)	23.73 (24.13)
Solid yield (%)	–	59.90
EY (%)	–	70.22
Geometric mean diameter (mm)	0.53	0.43
FR	0.15	1.19
CI (MJ/kg)	149.43	21.93
VI (MJ/kg)	17.39	13.44
Angle of repose (degree)	38.89	35.75
HR	1.29	1.21
CCI	22.48	17.35
C	0.40	0.35
Bulk density (kg/m^3)	231.45	193.48
Tapped density (kg/m^3)	300.71	235.67
Particle density (kg/m^3)	1251	1156
BET surface area (m^2/g)	–	0.9703
Pore volume (cm^3/g)	–	0.0015
Mean pore diameter (nm)	–	13.69

3.5. Fuel and flow properties of torrefied biomass

Table 2 presents the combustion indices of the biomass, which are commonly used as crucial parameters in thermochemical conversion processes. In coal-firing power plants, the recommended value of FR is between 0.5 and 3.0. The FR for RB and TB252-60-5 are 0.15 and 1.19, respectively. With increase in temperature, FR of RB increases since fixed carbon content increases along with decrease in volatile matter. The fuel having higher FR leads to increase in unburnt portion of the fuel, which decreases boiler efficiency during the operation. The fuel which has FR greater than 2 can cause ignition and flammability problem during the application. The reported range of CI and VI for coal are: CI should be less than 23 MJ/kg and VI should be greater than 14.5 MJ/kg [36]. The calculated value of CI and VI for RB are 149.43 MJ/kg and 17.39 MJ/kg, respectively. This shows that RB should not be used as an alternative fuel without prior treatment. After torrefaction, CI and VI for TB252-60-5, are 21.93 and 13.44, respectively. Transportation and handling are noteworthy processes which involve during the conversion process of biomass. These processes are extremely influenced by flowing ability of biomass. The materials having angle of repose between 31 and 35° have good flowing property and between 25 and 30° have excellent flowing property, materials having HR between 1.19 and 1.25 have fair-flowing properties and between 1.12 and 1.18 have good flowing properties [34], materials having CCI between 11 and 15, 16–20 and 21–25 have good, fair and passable flow behavior, respectively [34,35]. The angle of repose for RB and TB252-60-5 are 38.39, and 35.75, respectively. HR and CCI are important parameters which depict flow behavior of material. The calculated value of HR for RB and TB252-60-5 are 1.29 and 1.21, respectively. CCI is a measure of bulk density, tapped density, moisture content, surface area and cohesiveness of biomass since it varies with all these parameters. CCI of RB and TB252-60-5 are 22.48 and 17.35, respectively. RB torrefied at higher temperature has lesser tendency of agglomeration than the RB, leading to better flow property. The flowing property of biomass can also be explained by cohesive forces (between the particles) and friction forces (between the wall and the particles) [35]. The cohesion coefficient of RB and TB252-60-5 are 0.40 and 0.35, respectively, which shows that after torrefaction cohesive force between the particle decreases, which favors the flowing behavior of TB. This shows that fuel and flow properties of TB moving toward the properties of coal, which makes it suitable as an alternative source of solid fuel or it, can be blend with coal.

3.6. BET surface area and density of raw and torrefied biomass

The surface area, pore diameter and pore volume of were obtained using the BET method. BET surface area, pore diameter and pore volume of TB252-60-5 were found to be 0.9703 m^2/g, 13.69 nm and 0.0015 cm^3/g, respectively. Similar results were reported by Doddapaneni et al. [37] and Granados et al. [38]. The variation of density of RB and TB252-60-5 are presented in Table 2. It was noticed that all three types of densities (bulk, tapped and particle) decreased as the temperature increased during torrefaction. The bulk, tapped and particle densities of RB were 231.45, 300.71, and 1251 kg/m^3, respectively; and for TB252-60-5, they

were 193.48, 235.67, and 1156 kg/m^3, respectively. The release of volatile matter from RB at higher temperature creates inside voids, which causes decrease in density along with increase in porosity of TB. The TB with increased surface area can be used as an adsorbent in many processes. Conag et al. [22] investigated the bulk and tapped density of switchgrass, sugarcane bagasse and sugarcane leaves. They found that bulk density of switchgrass varied from 50 to 264 kg/m^3 and bulk density of torrefied switchgrass varied from 68 to 325 kg/m^3 whereas bulk and tapped density of sugarcane bagasse varies from 46 to 87 kg/m^3 and 65–125 kg/m^3, respectively.

3.7. Thermogravimetric analysis

Fig. 4 (a and b) show the TGA and DTG analyses of RB and TB252-60-5. Each component of biomass (hemicellulose, cellulose and lignin) shows different thermal behavior; hence, they have different thermal degradation temperature. Hemicellulose and cellulose degraded at lower temperature between 200 and 350 °*C*, while lignin decomposes at a wider temperature range between 280 and 600 °*C* [39]. Major mass loss in case of hemicellulose and cellulose occurs between 268 °*C* to 355 °*C* [40]. Fig. 4 (a and b) show that entire thermal degradation process can be divided into three zones viz. drying (1st zone), devolatilization (2nd zone) and char formation (3rd zone). Drying zone corresponds to removal of moisture and light volatile matter whereas devolatilization zone corresponds to active pyrolysis of RB or TB. In char formation zone, disruption and demethylation of lignin leads to char formation [41]. As a representative case, 20% mass loss was observed for RB at around 290 °*C*; whereas, for TB, it was observed at 353 °*C*. This shift in decomposition temperature may be attributed to lower amount of hemicellulose present in TB. The char yield in case of RB is 21%, however in case of TB252-60-5; char yield is 47%. This increase in char yield is also attributed to the decomposition of hemicellulose and limited decomposition of cellulose during torrefaction. The shoulder appeared in the DTG curve revealed decomposition of hemicellulose in case of RB and generally, it was observed at around 300 °*C* [42]. In this study, similar shoulder can be seen in Fig. 4 (b) for RB. In case of TB252-60-5, shoulder disappeared, confirming that hemicellulose has already been degraded during torrefaction. Yang et al. [40] illustrated that peaks appeared in DTG curve with maximum weight loss, conforming the presence of cellulose in the biomass. The peaks in DTG curve for RB and TB can be seen at temperature around 360 °*C*. Comparing RB and TB252-60-5, the intensity of peak in case of TB252-60-5 is lower, confirming the degradation of cellulose in this range of temperature.

3.8. Fourier transform infrared spectroscopy (FTIR)

FTIR analysis was performed to observe the chemical changes in biomass due to torrefaction (Fig. 5). The structural and chemical changes in biomass are mainly due to decomposition of hemicellulose, which occurs mainly in the range of 200 °*C* to 300 °*C*. In the wave number range from 4000 to 400 cm^{-1}, the functional groups of concern are O-H, C=O, C=C, C-H, and C-O-C. The characteristic peak between 3400 and 3100 cm^{-1} corresponds to stretching vibration of O-H bond [43] present mainly due to intra and intermolecular hydrogen bonding between alcoholic and phenolic groups present in cellulose and hemicellulose of biomass [44]. It can be observed that intensity of O-H bond in TB250-60-5 has decreased due to torrefaction. Decrease in O-H bond intensity inferred disruption of hemicellulose during torrefaction. The decrease in intensity of peak between 2900 and 2750 cm^{-1} confirms the decrease of C-H bond stretching of aliphatic groups such as methyl and methelene compounds associated with alkanes and alkenes present in RB [45]. Decrease in intensity of peaks between 1750 and 1500 cm^{-1} may be attributed to deacetylation reaction, which causes decomposition of ester group present in hemicellulose [46]. Between wave number of 600–700 cm^{-1}, intensity of peaks shows the presence of single and cyclic group of aromatic compound [47]. Thus, as the process temperature increases, the intensity of peaks decreases for TB252-60-5 in comparison to RB, conforming structural change of chemical compounds present in RB like water molecules, carboxyl groups, esters, aldehydes, ketones, acids and aromatic compounds.

3.9. Scanning electron microscope (SEM) and energy dispersive X-ray (EDX) analysis

To understand the influence of torrefaction on morphology of biomass, the scanning electron microscope images of RB and TB252-60-5 with 5000 magnification are presented in Fig. 6. The impact of thermal pretreatment could be seen in Fig. 6 (c). Generally, hemicelluloses are branched polysaccharides which contain strong bulky and branched tissues of xylem [48]. Branched structure on the surface of the RB elucidates the presence of hemicellulose (Fig. 6 (a)). However, in case of TB, these branched structures started disappearing, suggesting degradation of hemicellulose during torrefaction. The presence of pores is clearly visible for TB252-60-5. The generation of pores in case of TB252-60-5 is attributed to lower particle density than RB, which may decrease the grinding energy requirement for size reduction of RB and increase in surface area. These are in agreement with the results

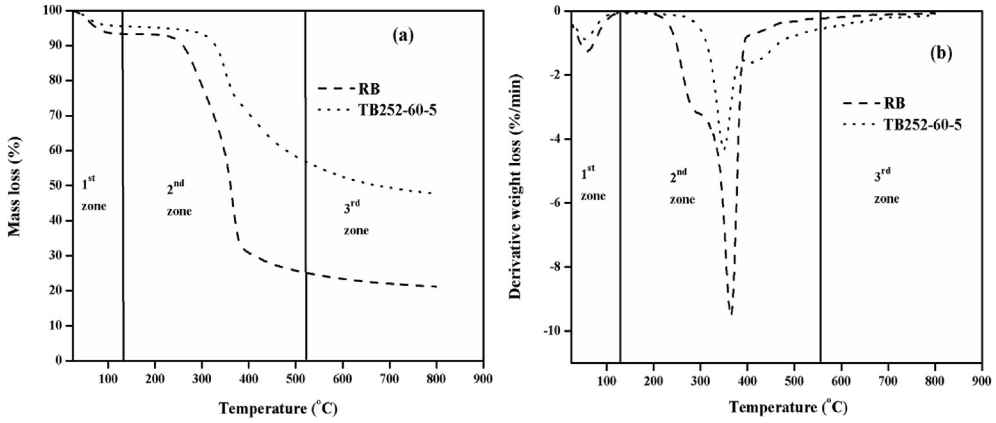

Fig. 4. Thermogravimetric analysis of RB and TB252-60-5 (a) TGA (b) DTG.

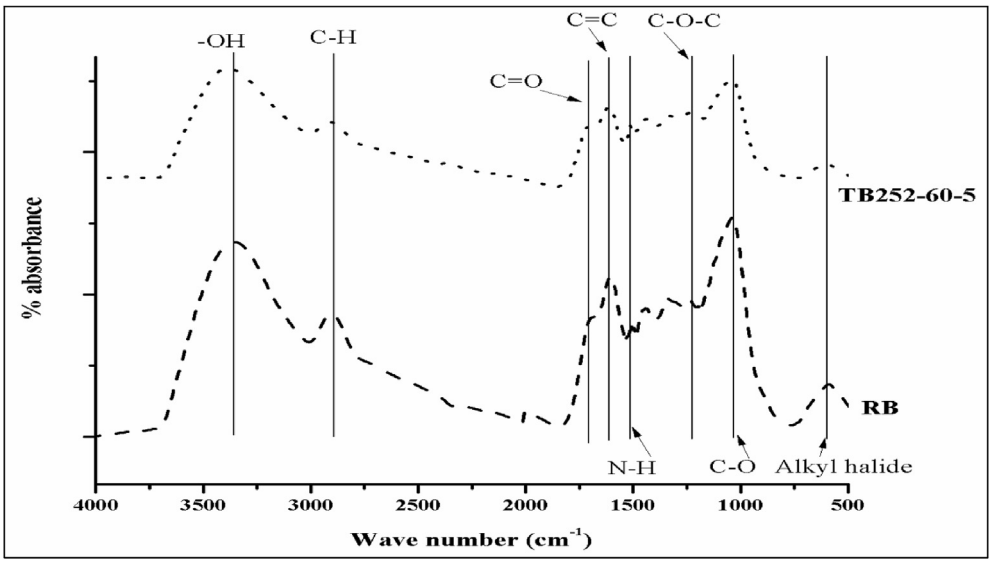

Fig. 5. FTIR spectra of RB and TB252-60-5.

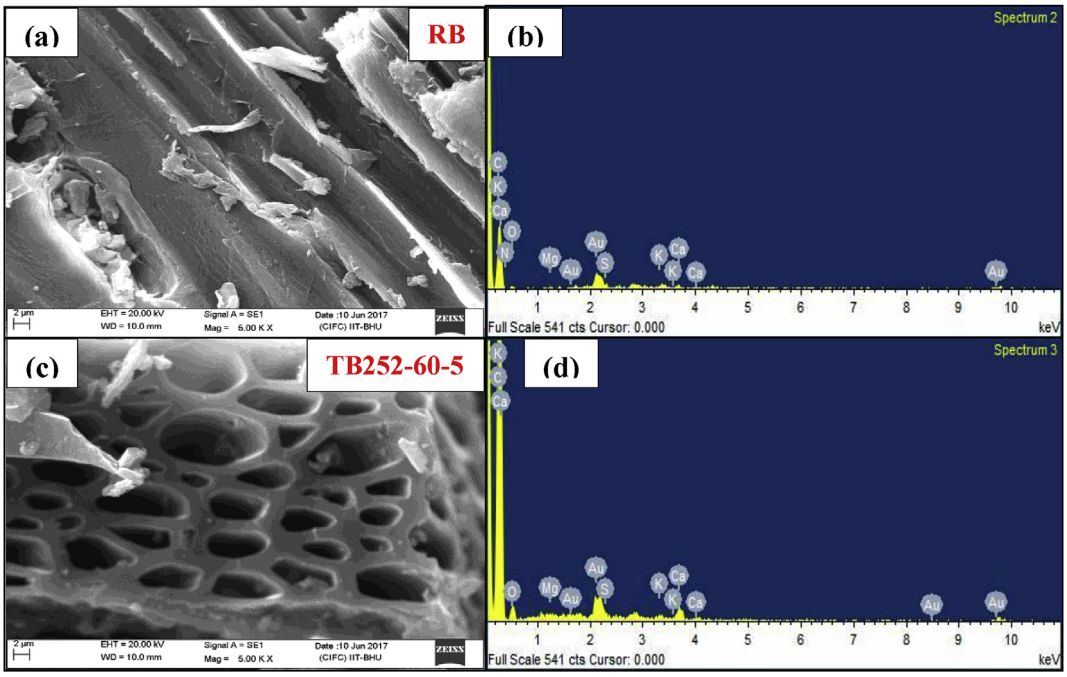

Fig. 6. SEM and EDX images: (a) and (b) for RB, (c) and (d) for TB252-60-5.

reported by Ibrahim et al. [48], Bach et al. [49].

Energy dispersive X-ray analysis is used to detect chemical elements present in the sample and to approximate their relative abundance. The EDX images of RB and TB252-60-5 are shown in Fig. 6 (b and d). It can be observed that in case of TB252-60-5, some useful elements like Nitrogen (N), Calcium (Ca), Magnesium (Mg) and Potassium (K) appear with higher peak intensity along with Carbon (C) and Oxygen (O) than RB indicating densification due to torrefaction. Oxygen gets reduced due to removal of −OH bonds, which is also supported by the FTIR analysis (Fig. 5). The increase in carbon content is also supported by enhanced fixed carbon content due to torrefaction, as presented in Table 2.

3.10. X-ray diffraction (XRD) analysis

The major components of biomass are hemicellulose, cellulose and lignin. Among these, hemicellulose and lignin are amorphous in nature and cellulose is crystalline [50]. To investigate the effect of torrefaction on crystalline nature of RB and TB252-60-5, XRD analysis was performed and crystallinity index (CrI), FWHM of (002) peak and crystal size (L_{002}) were also calculated. The results are shown in Fig. 7 and Table 3.

At $2\theta = 22°$, the strongest peak with highest intensity originated from 002 crystalline plane. It was observed that relative peak intensity of TB252-60-5 is lower than the RB. This shows that crystallinity of biomass decreased after torrefaction. Also, CrI of RB and

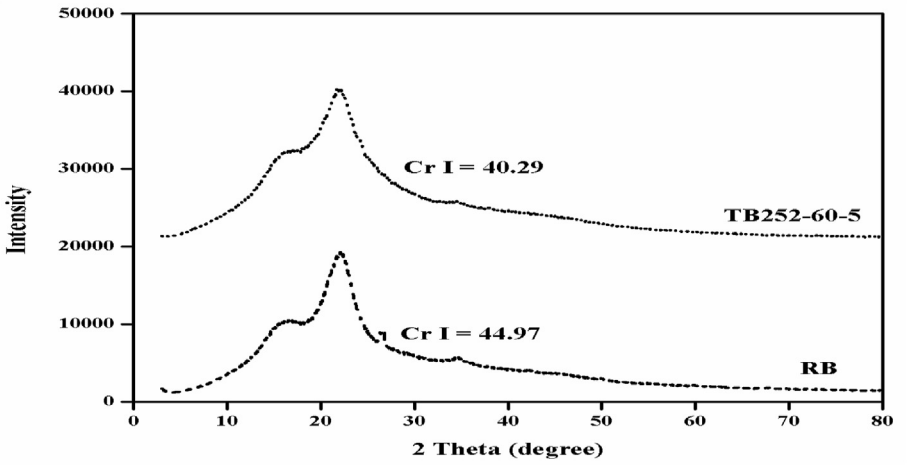

Fig. 7. XRD spectra of RB and TB252-60-5.

Table 3
Crystalline parameters of RB and TB252-60-5.

Sample	CrI (%)	2θ (degree)		β[a](degree)	L_{002} (nm)
		I_{002}	I_{am}		
RB	44.97	21.8	14.9	9.7	0.87
TB252-60-5	40.29	21.7	14.5	11.5	0.73

[a] Full width at half maximum (FWHM) of (002) peak.

TB252-60-5 was found to be 44.97 and 40.29%, respectively, which confirm the decrease in crystallinity. The decrease in crystallinity might be due to disruption of intermolecular hydrogen bonding [51] and degradation of cellulose during torrefaction. FWHM of (002) peak increases in case of TB252-60-5 with respect to RB. The crystal size decreases in case of TB252-60-5. Thus the crystal size of biomass decreases upon torrefaction. Similar results were obtained many researchers. Zheng et al. [50] investigated the effect of torrefaction on crystalline behavior of corncob. They found that, at mild torrefaction, CrI of torrefied corncob increased, while at severe torrefaction CrI decreased due to degradation of crystalline cellulose of corncob. Similar results were also obtained by Wen et al. [52] during torrefaction of Bamboo.

3.11. Moisture absorption

Fig. 8 shows the percentage of moisture absorbed by RB and TB252-60-5. RB and TB252-60-5 absorbed 8.15 and 4.51% moisture, respectively from open environment (average relative humidity of 60% ±3) when kept for one day. After 5 days, percentage of moisture absorbed by RB, and TB252-60-5 are 34.44, and 7.12%, respectively. The water absorption capacity of biomass is associated with the amount of hemicellulose present in biomass. Hemicellulose contains many hydroxyl group (-OH) which compel biomass to be polar and form hydrogen bonds with water molecules easily. Due to torrefaction, hydroxyl bonds (-OH) in biomass are dissociated and became unsaturated having non-polar characteristics, which diminishes the attraction of biomass to form hydrogen bonds with water molecules [49]. TB252-60-5 may also absorb less moisture due to deposition of tar, condensing on the surface [36]. Tar deposition prevents the capillary rise of water molecules due to blockage of pores inside TB252-60-5. The torrefaction makes biomass hydrophobic so that it engrosses lesser moistness and

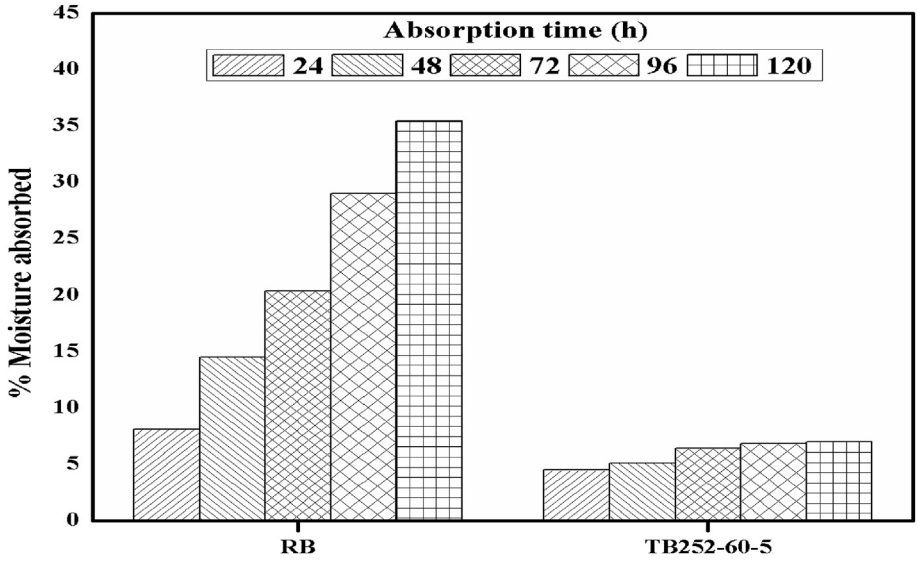

Fig. 8. Moisture absorption characteristics of RB and TB252-60-5.

offers more stability to biomass when kept in open environment. This suggests that TB obtained at higher temperature can be stored like coal in open environment, which significantly reduces transport, storage and handling cost of biomass.

4. Conclusions

The torrefaction of *Acacia nilotica* was carried out in a laboratory scale fixed-bed reactor. The process parameters like temperature, residence time and heating rate were optimized for HHV and EY. A different set of parameters were obtained in case of optimum HHV and EY of TB individually. The optimum value of temperature, residence time and heating rate to obtain maximum value of HHV and EY combined, were 252 °C, 60 min, and 5 °C/min, respectively. It was noted that the effect of temperature on torrefaction was significant, while effect of residence time and heating rate were minimal. Besides, the physical and chemical properties of RB improved due to torrefaction. For example, MC, H/C ratio and O/C ratio decreased by 73.23, 52.94 and 46.22%, respectively; whereas FC content and HHV increased by 75.54 and 18.62%, respectively. FR increased by 87.39%; whereas, CI and VI decreased by 83.32 and 22.71%, respectively. Flow properties such as angle of repose, HR, CCI and cohesion coefficient (C) decreased by 8.04, 6.20, 22.48, and 12.5%, respectively. Bulk, tapped and particle densities of TB252-60-5 were decreased by 16.4, 21.62 and 7.59%, respectively. Moisture sorption test confirmed that TB252-60-5 absorbed 27.32% less moisture than RB when kept in open environment at comparable relative humidity. TGA study suggests that onset of devolatilization shifted to higher temperature in case of TB and char yield increased during pyrolysis of TB. Torrefaction has greatly enhanced surface defects and reduced crystallinity of biomass as revealed by SEM-EDX and XRD analysis individually.

Overall, it may be concluded that optimization of torrefaction process favors two aspects; first, it may reduce the operational cost during the scaling of process at industrial level. Secondly, TB has much improved properties than RB, which can increase the process efficiency during its utilization in pyrolysis, gasification and co-pyrolysis with coal in thermal power plants.

Acknowledgement

The authors acknowledge the funding from Science and Engineering Research Board (SERB), New Delhi, Indian through fund no. SR/FTP/ETA-56/2012.

Appendix A. Supplementary data

Supplementary data to this article can be found online at https://doi.org/10.1016/j.energy.2019.115865.

References

[1] Zhang Y, Song K. Thermal and chemical characteristics of torrefied biomass derived from a generated volatile atmosphere. Energy 2018;165:235–45.
[2] Gong S-H, Im H-S, Um M, Lee H-W, Lee J-W. Enhancement of waste biomass fuel properties by sequential leaching and wet torrefaction. Fuel 2019;239:693–700.
[3] Nazari L, Yuan Z, Ray MB, Xu C. Co-conversion of waste activated sludge and sawdust through hydrothermal liquefaction: optimization of reaction parameters using response surface methodology. Appl Energy 2017;203:1–10.
[4] Shahbaz M, Yusup S, Inayat A, Patrick DO, Pratama A. Application of response surface methodology to investigate the effect of different variables on conversion of palm kernel shell in steam gasification using coal bottom ash. Appl Energy 2016;184:1306–15.
[5] Gonçalves da Silva C. Renewable energies: Choosing the best options. Energy 2010;35(8):3179–93.
[6] Zhang S, Su Y, Xu D, Zhu S, Zhang H, Liu X. Effects of torrefaction and organic-acid leaching pretreatment on the pyrolysis behavior of rice husk. Energy 2018;149:804–13.
[7] Lee J-W, Kim Y-H, Lee S-M, Lee H-W. Optimizing the torrefaction of mixed softwood by response surface methodology for biomass upgrading to high energy density. Bioresour Technol 2012;116:471–6.
[8] Wannapeera J, Worasuwannarak N. Upgrading of woody biomass by torrefaction under pressure. J Anal Appl Pyrolysis 2012;96:173–80.
[9] Trubetskaya A, Leahy JJ, Yazhenskikh E, Müller M, Layden P, Johnson R. Characterization of woodstove briquettes from torrefied biomass and coal. Energy 2019;171:853–65.
[10] Rousset P, Davrieux F, Macedo L, Perré P. Characterisation of the torrefaction of beech wood using NIRS: combined effects of temperature and duration. Biomass Bioenergy 2011;35(3):1219–26.
[11] Álvarez A, Nogueiro D, Pizarro C, Matos M, Bueno JL. Non-oxidative torrefaction of biomass to enhance its fuel properties. Energy 2018;158:1–8.
[12] Dai L, Wang Y, Liu Y, Ruan R, He C, Yu Z. Integrated process of lignocellulosic biomass torrefaction and pyrolysis for upgrading bio-oil production: a state-of-the-art review. Renew Sustain Energy Rev 2019;107:20–36.
[13] Park J, Meng J, Lim KH, Rojas OJ, Park S. Transformation of lignocellulosic biomass during torrefaction. J Anal Appl Pyrolysis 2013;100:199–206.
[14] Dacres OD, Tong S, Li X, Zhu X, Edreis EMA, Liu H. Pyrolysis kinetics of biomasses pretreated by gas-pressurized torrefaction. Energy Convers Manag 2019;182:117–25.
[15] Asadullah M, Adi AM, Suhada N, Malek NH, Saringat MI, Azdarpour A. Optimization of palm kernel shell torrefaction to produce energy densified biocoal. Energy Convers Manag 2014;88:1086–93.
[16] Bach Q–V, Gye H–R, Song D, Lee C–J. High quality product gas from biomass steam gasification combined with torrefaction and carbon dioxide capture processes. Int J Hydrogen Energy. https://doi.org/10.1016/j.ijhydene.2018.11.237
[17] Louwes AC, Basile L, Yukananto R, Bhagwandas JC, Bramer EA, Brem G. Torrefied biomass as feed for fast pyrolysis: an experimental study and chain analysis. Biomass Bioenergy 2017;105:116–26.
[18] Deng J, Wang G-j, Kuang J-h, Zhang Y-l, Luo Y-h. Pretreatment of agricultural residues for co-gasification via torrefaction. J Anal Appl Pyrolysis 2009;86(2):331–7.
[19] Hanoğlu A, Çay A, Yanık J. Production of biochars from textile fibres through torrefaction and their characterization. Energy 2019;166:664–73.
[20] Buratti C, Barbanera M, Lascaro E, Cotana F. Optimization of torrefaction conditions of coffee industry residues using desirability function approach. Waste Manag 2018;73:523–34.
[21] Phanphanich M, Mani S. Impact of torrefaction on the grindability and fuel characteristics of forest biomass. Bioresour Technol 2011;102(2):1246–53.
[22] Conag AT, Villahermosa JER, Cabatingan LK, Go AW. Energy densification of sugarcane bagasse through torrefaction under minimized oxidative atmosphere. J Environ Chem Eng 2017;5(6):5411–9.
[23] Chen W-H, Lin B-J, Colin B, Pétrissans A, Pétrissans M. A study of hygroscopic property of biomass pretreated by torrefaction. Energy Procedia 2019;158:32–6.
[24] Chen W-H, Kuo P-C. Torrefaction and co-torrefaction characterization of hemicellulose, cellulose and lignin as well as torrefaction of some basic constituents in biomass. Energy 2011;36(2):803–11.
[25] Mundike J, Collard F-X, Görgens JF. Torrefaction of invasive alien plants: influence of heating rate and other conversion parameters on mass yield and higher heating value. Bioresour Technol 2016;209:90–9.
[26] Dhanavath KN, Shah K, Bankupalli S, Bhargava SK, Parthasarathy R. Derivation of optimum operating conditions for the slow pyrolysis of Mahua press seed cake in a fixed bed batch reactor for bio–oil production. J Environ Chem Eng 2017;5(4):4051–63.
[27] Gholami A, Pourfayaz F, Hajinezhad A, Mohadesi M. Biodiesel production from Norouzak (Salvia leriifolia) oil using choline hydroxide catalyst in a microchannel reactor. Renew Energy 2019;136:993–1001.
[28] Cotana F, Buratti C, Barbanera M, Lascaro E. Optimization of the steam explosion and enzymatic hydrolysis for sugars production from oak woods. Bioresour Technol 2015;198:470–7.
[29] Garg R, Anand N, Kumar D. Pyrolysis of babool seeds (Acacia nilotica) in a fixed bed reactor and bio-oil characterization. Renew Energy 2016;96:167–71.
[30] Tan IAW, Ahmad AL, Hameed BH. Optimization of preparation conditions for activated carbons from coconut husk using response surface methodology. Chem Eng J 2008;137(3):462–70.
[31] Gratuito MK B, Panyathanmaporn T, Chumnanklang RA, Sirinuntawittaya N, Dutta A. Production of activated carbon from coconut shell: optimization using response surface methodology. Bioresour Technol 2008;99:4887–95.
[32] Tooyserkani Z, Sokhansanj S, Bi X, Lim J, Lau A, Saddler J. Steam treatment of four softwood species and bark to produce torrefied wood. Appl Energy 2013;103:514–21.
[33] Cai J, He Y, Yu X, Banks SW, Yang Y, Zhang X. Review of physicochemical properties and analytical characterization of lignocellulosic biomass. Renew Sustain Energy Rev 2017;76:309–22.
[34] Lumay G, Boschini F, Traina K, Bontempi S, Remy JC, Cloots R. Measuring the flowing properties of powders and grains. Powder Technol 2012;224:19–27.
[35] Szalay A, Kelemen A, Pintye-Hódi K. The influence of the cohesion coefficient (C) on the flowability of different sorbitol types. Chem Eng Res Des 2015;93:349–54.
[36] Ohm T-I, Chae J-S, Kim J-K, Oh S-C. Study on the characteristics of biomass for co-combustion in coal power plant. J Mater Cycles Waste Manag 2015;17(2):

249–57.
[37] Doddapaneni TRKC, Jain R, Praveenkumar R, Rintala J, Romar H, Konttinen J. Adsorption of furfural from torrefaction condensate using torrefied biomass. Chem Eng J 2018;334:558–68.
[38] Granados DA, Basu P, Chejne F, Nhuchhen DR. Detailed investigation into torrefaction of wood in a two-Stage inclined rotary torrefier. Energy Fuels 2017;31(1):647–58.
[39] Ren S, Lei H, Wang L, Bu Q, Chen S, Wu J. Thermal behaviour and kinetic study for woody biomass torrefaction and torrefied biomass pyrolysis by TGA. Biosyst Eng 2013;116(4):420–6.
[40] Yang H, Yan R, Chen H, Lee DH, Zheng C. Characteristics of hemicellulose, cellulose and lignin pyrolysis. Fuel 2007;86(12):1781–8.
[41] Collard F-X, Blin J. A review on pyrolysis of biomass constituents: Mechanisms and composition of the products obtained from the conversion of cellulose, hemicelluloses and lignin. Renew Sustain Energy Rev 2014;38:594–608.
[42] Müller-Hagedorn M, Bockhorn H, Krebs L, Müller U. A comparative kinetic study on the pyrolysis of three different wood species. J Anal Appl Pyrolysis 2003;68–69:231–49.
[43] Gan YY, Ong HC, Ling TC, Chen W-H, Chong CT. Torrefaction of de-oiled Jatropha seed kernel biomass for solid fuel production. Energy 2019;170:367–74.
[44] Singh Rk, Sarkar A, Chakraborty JP. Effect of torrefaction on the physico-chemical properties of pigeon pea stalk (Cajanus cajan) and estimation of kinetic parameters. Renew Energy 2019;138:805–19.
[45] He Q, Ding L, Gong Y, Li W, Wei J, Yu G. Effect of torrefaction on pinewood pyrolysis kinetics and thermal behavior using thermogravimetric analysis. Bioresour Technol 2019;280:104–11.
[46] Carrasco F, Roy C. Kinetic study of dilute-acid prehydrolysis of xylan-containing biomass. Wood Sci Technol 1992;26(3):189–208.
[47] Gomez-Serrano V, Pastor-Villegas J, Perez-Florindo A, Duran-Valle C, Valenzuela-Calahorro C. FT-IR study of rockrose and of char and activated carbon. J Anal Appl Pyrolysis 1996;36(1):71–80.
[48] Ibrahim RHH, Darvell LI, Jones JM, Williams A. Physicochemical characterisation of torrefied biomass. J Anal Appl Pyrolysis 2013;103:21–30.
[49] Bach Q-V, Skreiberg Ø. Upgrading biomass fuels via wet torrefaction: a review and comparison with dry torrefaction. Renew Sustain Energy Rev 2016;54:665–77.
[50] Zheng A, Zhao Z, Chang S, Huang Z, Zhao K, Wei G. Comparison of the effect of wet and dry torrefaction on chemical structure and pyrolysis behavior of corncobs. Bioresour Technol 2015;176:15–22.
[51] Wannapeera J, Worasuwannarak N. Examinations of chemical properties and pyrolysis behaviors of torrefied woody biomass prepared at the same torrefaction mass yields. J Anal Appl Pyrolysis 2015;115:279–87.
[52] Wen J-L, Sun S-L, Yuan T-Q, Xu F, Sun R-C. Understanding the chemical and structural transformations of lignin macromolecule during torrefaction. Appl Energy 2014;121:1–9.